Computers in Biology and Medicine 191 (2025) 110110

Contents lists available at ScienceDirect

Computers in Biology and Medicine

journal homepage: www.elsevier.com/locate/compbiomed

Interpretable deep learning method to predict wound healing progress based on collagen fibers in wound tissue

Juan He [a,b,1], Xiaoyan Wang [c,1], Zhengshan Wang [a], Ruitao Xie [b], Zhiming Zhang [c], Tzu-Ming Liu [c], Yunpeng Cai [b,*], Long Chen [a]

[a] Department of Computer and Information Science, Faculty of Science and Technology, University of Macau, 999078, Macau
[b] Shenzhen Institute of Advanced Technology, Chinese Academy of Sciences, Shenzhen, 518055, China
[c] Institute of Translational Medicine, Faculty of Health Sciences & Ministry of Education Frontiers Science Center for Precision Oncology, University of Macau, 999078, Macau

ARTICLE INFO

Keywords:
Wound healing
Fine-tune VGG16 model
Visual interpretable framework

ABSTRACT

Background and objective: The dynamic evolution of collagen fibers during wound healing is crucial for assessing repair progression, guiding clinical treatment, and drug screening. Current quantitative methods analyzing collagen spatial patterns (density, orientation variance) lack established criteria to both stratify distinct healing periods and detect delayed healing conditions, necessitating the establishment of a novel classification method for wound healing status based on collagen fibers.

Methods: We propose a deep learning method to classify various time points of wound healing and delayed healing using histological images of skin tissue. We fine-tune a pre-trained VGG16 model and enhance it with an interpretable framework that combines LayerCAM and Guided Backpropagation, leveraging model gradients and features to visually identify the tissue regions driving model predictions.

Results: Our model achieved 85 % accuracy in a five-class classification task (normal skin, wound skin at 0, 3, 7, and 10 days) and 78 % in a three-class task (normal skin, wound skin at 0 days, diabetic wound skin at 10 days). Our interpretable framework accurately localizes collagen fibers without pixel-level annotations, demonstrating that our model classifies healing periods and delayed healing based on collagen regions in histological images rather than other less relevant tissue structures.

Conclusions: Our deep learning method leverages collagen fiber features to predict various time points of wound healing and delayed healing with high accuracy and visual interpretability, enhancing doctors' trust in model decisions. This could lead to more precise and effective wound treatment practices.

1. Introduction

During the skin wound healing process, the dynamic changes of collagen fibers play a central biological role. Precise monitoring of these changes is crucial for assessing the progress of wound healing and provides essential guidance for the formulation of clinical treatment strategies and drug screening [1]. However, traditional quantitative analysis methods mainly focus on measuring spatial properties such as the density and orientation of collagen fibers in wound histological images [2]. These methods have obvious deficiencies in determining the classification criteria for different wound healing periods and delayed healing because they lack clear threshold definitions. This not only makes it difficult to become a reliable gold standard for distinguishing wound healing statuses but also poses a challenge to accurately predicting the wound healing progress. Deep learning models are able to identify and analyze complex patterns and subtle differences that are difficult to detect with traditional methods. They show great potential and prospects in capturing the subtle features of collagen fibers in histological images of wound tissue, thereby hopefully improving the accuracy of predicting wound healing statuses.

When studying collagen fibers in wound tissue histological images, traditional analysis techniques primarily emphasize the quantification of the spatial structural characteristics of collagen. These characteristics play an important auxiliary role in identifying and describing wound

* Corresponding author.
E-mail address: yp.cai@siat.ac.cn (Y. Cai).
[1] These authors contribute equally to this work.

https://doi.org/10.1016/j.compbiomed.2025.110110
Received 27 September 2024; Received in revised form 23 March 2025; Accepted 27 March 2025
Available online 7 April 2025

tissue [3–8]. Specifically, Liu et al. proposed innovative computational methods that achieve quantitative analysis of collagen through curve transformation [6]. Clemons introduced a method for collagen orientation assessment, revealing differences in the coherency of collagen fibers between normal and scar tissue [7]. It is important to highlight that while current research has shown significant differences in collagen spatial orientation and density between normal and wound tissues, there is a lack of significant differences among different periods of wound healing [8]. Consequently, it becomes increasingly challenging to establish pathological threshold values associated with collagen characteristics to differentiate between different periods of wound healing. This limitation renders traditional methods inadequate for effectively classifying wounds of various statuses.

Deep learning drives significant breakthroughs and innovations in the healthcare industry [9–13]. Currently, several deep learning models have achieved high-precision classification of normal and scar tissues based on collagen fibers in wound histological images [14,15]. However, scars are already-healed wound tissues, and they did not explore the different periods of the wound healing process. In addition, in their study, the researchers selected a subset of feature maps from the mode layers to extract collagen fibers and perform further analysis. However, they did not provide a clear explanation of the feature selection mechanism. This lack of clarity restricts these models to be applied to other datasets. Additionally, images of wound surfaces are utilized in deep learning models to predict various stages of wound healing [17] or to assess and forecast healing and infection status [16]. These images often contain background information unrelated to the healing state, such as uninjured skin, which may impact the model's accuracy. Moreover, existing studies frequently overlook the relationship between the internal structures of the wound, such as collagen fibers, and the healing status. Currently, research utilizing deep learning models to predict different statuses of wound healing based on collagen fiber images remains limited. Therefore, we aim to explore and develop a deep learning method for assessing wound healing status based on collagen fibers, with the goal of enhancing our understanding and potentially achieving a more comprehensive and accurate evaluation of wound healing progress.

However, due to the limited availability of histological images from wound tissue in the real world, it is challenging to directly train a powerful deep learning model. To overcome this challenge, transfer learning has emerged as an effective approach. Specifically, transfer learning involves training a powerful model on a similar task and then fine-tuning the model to adapt it to the target task [18,19]. In this paper, we apply the pre-trained VGG16 [20] deep learning model, which was initially trained on the ImageNet dataset [21], to achieve the classification of wound healing progress through a process known as fine-tuning. The pre-trained VGG16 model has learned rich feature representations on ImageNet, and through transfer learning, we can leverage these generic features to accelerate the learning process for the classification of wound healing progress.

Accurate localization of collagen in wounds is an important component of wound healing diagnosis, but there is currently a paucity of collagen localization and segmentation models trained on annotated data, primarily due to a lack of sufficient annotated samples. Therefore, seeking breakthrough methods to solve this bottleneck problem is crucial for promoting the development of clinical practice. This study proposes an interpretable collagen localization technique, which not only realizes the visualization of the model's decision-making process but also accurately locates the collagen in the wound, even in the absence of pixel-level annotations. This visualizable interpretable framework integrates LayerCAM [22] and Guided Backpropagation algorithms [23]. LayerCAM is an extension of the visual interpretability technique of Class Activation Mapping (CAM) [24]. Through strategic weighting and integration of model features, LayerCAM effectively activates the regions corresponding to collagen fibers in the histological images of wound tissue, which allows us to overcome the limitations of data annotation and accurately locate the spatial distribution of collagen, even without detailed annotations. Meanwhile, Guided Backpropagation provides fine-grained information on the critical pixels of collagen through a special backpropagation mechanism [23]. Furthermore, this visualization provides evidence that our model assesses wound healing progression based on the collagen regions in the histological images rather than categorizing them based on other tissue structures, such as adipose tissue and blood vessels, whose structures and arrangements are less indicative of wound healing. This not only deepens our comprehension of the model's decision-making mechanisms but also underscores the significance of collagen fibers in the wound-healing journey.

We propose a visually interpretable deep learning classification model aimed at assessing wound healing progress using collagen fibers in wound histological images. This advancement tackles the limitations of conventional quantitative methods, which faced challenges in accurately discerning different statuses of wound healing using histological images alone. The main contributions of this paper are as follows:

(1) Two types of datasets related to skin wound healing were collected. The first type includes histological images of normal skin and wound skin at 0, 3, 7, and 10 days during the healing process. The second type comprises histological images of normal skin, wound skin at 10 days, and diabetic wound skin at 10 days.
(2) A deep learning classification model was developed to predict wound healing progress by fine-tuning a pre-trained VGG16 model.
(3) A visual interpretable framework that integrates LayerCAM and Guided Backpropagation algorithms was introduced. It not only realizes the visualization of the classification model's decision-making process but also accurately locates the collagen in wounds, even without pixel-level annotations.
(4) Traditional quantitative analysis methods were employed to calculate the directional coherency of collagen fibers in histological images of skin wounds at different healing time points and normal skin. T-tests were also used to assess significant differences in coherency among different skin categories. Furthermore, to compare with the proposed model, the coherency was incorporated as input into a support vector machine (SVM)-based classification model [25] to predict the progress of wound healing.

2. Related works

2.1. Collagen in wound healing

Collagen is crucial in wound healing, offering mechanical strength to the wound tissue, promoting cell migration and division, regulating intercellular communication, and supporting neovascularization [1,26].

After the injury, activated fibroblasts and myofibroblasts rapidly produce and secrete collagen, forming a dense and tough collagen fiber network in the wound area through cross-linking, providing structural support to stabilize the wound and providing a platform for cell movement [27,28].

For wound closure and the production of new tissue, the role of collagen is mainly reflected in enhancing the movement of cells in the wound area and promoting the growth of fibroblasts in adjacent areas, ultimately accelerating the healing process [29–31]. Moreover, collagen can interact with cell signaling pathways to regulate the cellular responses and inflammatory responses associated with healing [32–34].

Wound healing is accompanied by neovascularization, and collagen provides physical support and guidance for growth direction [35,36]. Part of the bioactive peptides in collagen activate the related signaling pathway by interacting with the receptor on the cell surface and promoting the proliferation and migration of vascular endothelial cells. This direct regulatory effect allows collagen to not only structurally support

neovascularization but also functionally promote the biological process of neovascularization [37–39].

Collagen is involved in the whole process of wound closure and tissue regeneration, and it is an important biomarker of wound healing. Based on the above understanding, we constructed a deep learning model to predict the degree of wound healing based on collagen images.

2.2. Deep learning for collagen analysis

In recent years, many deep learning models have been used to analyze collagen structures in biological tissues. The researchers predicted the elastic mechanical properties of tissues through deep learning based on second-harmonic generation (SHG) images of collagen [40]. Collagen fiber orientations in 2-D and 3-D images can also be identified and segmented by deep neural networks [41].

Multiple deep learning-based studies have revealed the link between collagen fibers and cancer development, so researchers are able to better understand the biological characteristics of cancer in-depth and also provide strong support for clinical decision-making. By combining a ridge filter with a deep neural network, the researchers successfully constructed a collagen fiber classifier based on breast cancer images [42]. In addition, the analysis of breast cancer pathology images by the convolutional neural network (CNN) revealed a very significant correlation between tissue stiffness and the presence of straight collagen fibers [43]. This finding adds a new strategy and direction to understanding breast cancer. Further, the researchers constructed the collagen fiber classifier collagenDL for colon cancer prediction based on the residual network, which can successfully predict the disease-free survival and overall survival rate of stage II-III colon cancer patients, enhancing the understanding of the prognosis of colon cancer [44].

Lee Y et al. developed a CNN model to classify scar tissue caused by burns based on collagen fibers, achieve precise differentiation of normal tissue from scar tissue, and quantitatively assess the microstructure of collagen [14,15]. Alan E. Woessner et al. trained a U-Net model that could accurately segment collagen-positive pixels, maintaining the corresponding segmentation performance even at different imaging depths [45]. Furthermore, Nicole Riberti et al. also successfully applied U-Net to characterize the complex microstructure of collagen bundles around dental implants according to specific directional properties of collagen bundles and to provide precise collagen segmentation and subsequent analysis [46].

Moreover, Park H et al. accurately extracted the center line of collagen fibers from histological images using deep neural networks. This enables comprehensive quantification of the spatial properties of collagen fibers, such as directionality, arrangement pattern, density, and length, and helps understand the microstructural features of collagen [47].

In general, the deep learning model further enriches the analysis and characterization methods of collagen fibers, provides more in-depth insights, can more accurately reveal the function and role of collagen fibers, and provides a scientific basis for the diagnosis and treatment of related diseases.

2.3. Deep learning for wound healing

The advancement of deep learning has brought a new revolution to the field of wound healing. This study categorizes deep learning-based wound healing analysis methods into two types: wound image segmentation and wound healing classification.

Research on wound image segmentation primarily relies on the U-Net architecture and its variants [48]. In specific application scenarios, researchers have proposed various innovative solutions: Changhan Wang's team developed an integrated deep learning system capable of simultaneous wound segmentation, infection detection, and healing prediction [49]; Kyle Quinn et al. designed a CNN model that achieves pixel-level segmentation of whole-slide H&E-stained wound sections within 30 s [2]; Chuanbo Wang implemented a lightweight MobileNetV2-based network for fully automated segmentation of foot ulcer images [50]. In microscopic imaging, Jake Jones successfully applied CNNs to automate the segmentation of skin tissue slices and in vivo label-free multiphoton microscopy (MPM) images [51], while Dilan Doğru's team developed enhanced U-Net architectures for high-precision segmentation across photobiomodulation [52] and in vitro wound microscopy imaging [53], demonstrating significant improvements in analysis time and sensitivity compared to ImageJ [54] and TScratch [55]. Furthermore, Maja Schlereth introduced deep learning for analyzing wound cross-sectional dimensions in ultrasound images [56].

Deep learning approaches for wound healing classification focus on assessing and predicting wound healing status. Key advancements include: Varun Shenoy et al.'s Deepwound system employing multi-label CNN to classify wound images and identify nine wound-related labels [57]; Héctor Carrión's HealNet utilizing self-supervised learning for stage progression prediction [16]; Lirong Wang's CNN-powered wound management model combined with multifunctional antibacterial hydrogels [17]; and Ramin Mousa et al. built a multi-modal AI model using transfer learning, combining Xception and GMRNN for precise classification of diabetic, pressure, surgical, and venous ulcers [58].

While existing U-Net-based wound segmentation methods require pixel-level annotations, the proposed framework achieves collagen region segmentation using only classification labels, substantially reducing manual annotation demands. Current deep learning approaches for wound healing classification predominantly analyze wound surface images containing extraneous backgrounds (e.g., healthy skin), whereas this study leverages histological wound interior imaging to enable precise characterization of critical tissue features like collagen fibers, thereby enhancing analytical accuracy.

3. Materials and methods

3.1. Materials

3.1.1. Animal model preparation

All animal experiments complied with the University of Macau's Sub-panel on Animal Research Ethics (UMARE - 019–2022). Male nude mice used for the experiments, aged between 6 and 8 weeks and weighed in a weight range of 20–23 g, were provided by the Animal Laboratory Facilities of the University of Macau. In this study, we used the excision wound splint model described by X. Wang (2019) [59]. First, each mouse was anesthetized, and then two full-thickness skin wounds with a diameter of 5 mm were created on both sides of the midline using a biopsy punch. Silicone splints surround each wound to keep its position stable, while the 3M Tegaderm dressing provides overlay protection. The damaged skin is extracted for histological examination at specific time intervals after the injury (e.g., day 0, 3, 7, 10).

Transgenic mice (B6. Cg-Lepob/J) were used were used to study chronic diabetic wounds. Following mating and breeding, the hybrid Lepob mice were identified. The ob + mice served as the control group, representing normal physiological conditions, while the ob/ob mice were considered diabetic. The skin wound model was implemented on both types of mice 12 weeks after breeding, using the same specific methodology as previously described.

3.1.2. Histological analysis using Masson's trichrome

Tissue specimens were fixed in 4 % paraformaldehyde, dehydrated in a graded ethanol series, and embedded in paraffin. For direct visualization of collagen fibers and histological assessment of collagen deposition, Masson trichrome staining (MT) was performed using the Kit (Heart Biological Technology). Optical photomicrographs were obtained at 40 × magnification (Hamamatsu NanoZoomer S60, 0.26 μm/pixel resolution) with a digital camera, using a consistent setting. In the histological images, the collagen fibers are mostly stained in blue,

whereas the appendages, such as hair follicles, sweat glands, and sebaceous glands, are stained in red or purple, as shown in Fig. 1.

3.1.3. Data processing

Through the aforementioned experiments, we obtained two datasets related to skin wound healing. The first dataset was collected from male nude mice and aims to assess the healing progress by examining changes in collagen fibers at different healing time points. This dataset includes five categories of histological images: normal skin (Control) and wound skin images taken at 0, 3, 7, and 10 days post-injury.

The second dataset was collected from B6 mice and consists of two batches collected, with the goal of identifying delayed healing due to diabetes. This dataset comprises histological images of normal skin (Control), wound skin at day 10 of healing, and diabetic wound skin at the same time point (Delay Day 10). Tables 1 and 2 provide statistical overviews of these two datasets, respectively. The bolded entry in Table 2 denote the cumulative counts of images per category across two data batches from Dataset 2.

To comprehensively evaluate the model's performance and effectively address potential overfitting issues associated with the random division of training and testing sets, this study adopted a five-fold cross-validation approach. A diagram of five-fold cross-validation is provided in the supplementary files. Specifically, the entire dataset was divided into five subsets. During each iteration of training, 80 % of the data was allocated to the training set, while the remaining 20 % served as the testing set. Importantly, the testing set in each iteration was unique, with no overlap across rounds, ensuring that every data point had an equal chance to be included in the testing set. This approach ensured that each sample contributed to the model evaluation process. As a result, the strategy significantly enhanced the reliability and robustness of the model assessment. The data partitioning results for Dataset 1 and Dataset 2 under the five-fold cross-validation are presented in Tables 3 and 4, respectively.

For the training set, we applied various data augmentation techniques, such as random flipping and rotation, to enhance data diversity and richness. To address the issue of imbalanced distribution between categories, we adjusted the class weights in the model's loss function. During training, higher weights were assigned to minority class samples, effectively reducing the impact of class imbalance on the loss function. To ensure compatibility with the VGG16 model, which requires input images of size 224 × 224, we used bilinear interpolation to resize all the images in our datasets to the desired dimensions.

Table 1
Data distributions of Dataset 1.

	Control	Day 0	Day 3	Day 7	Day 10
Dataset 1	28	12	15	31	38

Table 2
Data distributions of Dataset 2.

		Control	Day 10	Delay Day 10
Dataset 2	Batch 1	21	28	33
	Batch 2	23	44	33
	Sum	**44**	**72**	**66**

Table 3
Data splits of Dataset 1.

Data Splits		Control	Day 0	Day 3	Day 7	Day 10
1	Train	22	9	12	24	30
	Test	6	3	3	7	8
2	Train	22	9	12	25	30
	Test	6	3	3	6	8
3	Train	22	10	12	25	30
	Test	6	2	3	6	8
4	Train	23	10	12	25	31
	Test	5	2	3	6	7
5	Train	23	10	12	25	31
	Test	5	2	3	6	7

Table 4
Data splits of Dataset 2.

Data Splits		Control	Day 10	Delay Day 10
1	Train	35	57	52
	Test	9	15	14
2	Train	35	57	53
	Test	9	15	13
3	Train	35	58	53
	Test	9	14	13
4	Train	35	58	53
	Test	9	14	13
5	Train	36	58	53
	Test	8	14	13

3.2. Network architecture and training

Our overall framework is illustrated in Fig. 2. Initially, we collected two datasets of histological images of skin wound healing. Subsequently, we utilized these datasets to assess the state of wound healing based on the proposed CNN model and employed a visually interpretable framework to highlight the regions in the input images that contribute most significantly to the model's decision-making. Finally, for comparison with our proposed method, we used the traditional image analysis software ImageJ to quantitatively measure the coherency of collagen fibers in the histological images of wound tissue and input this coherency data into SVM to predict the progress of wound healing.

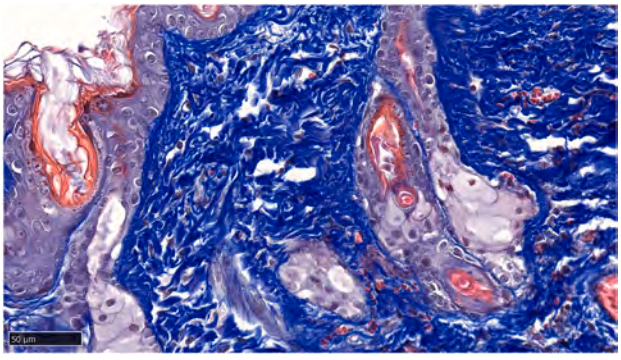

Fig. 1. Masson's trichrome-stained histological image of wound tissue. This histological image showcases blue-stained areas representing collagen fibers, while red or purple hues depict other structures such as hair follicles, sweat glands, and sebaceous glands.

3.2.1. Proposed CNN architecture

VGG16 is a widely adopted convolutional neural network architecture, which comprises 16 layers, including 13 convolutional layers and 3 fully connected layers. In this research, the pre-trained VGG16 model, initially trained on the ImageNet dataset, was utilized as the base architecture. Fine-tuning was conducted to adapt the model specifically for wound histological image classification. Specifically, considering the small size of our dataset, employing an overly large model could lead to overfitting. To address this issue, we chose to freeze the weights of the first seven convolutional layers of the pre-trained VGG16 model. This strategic choice was made to leverage the feature extraction capabilities of these initial layers, which are known to capture general image features that are beneficial for a wide range of tasks. By freezing their weights, we prevented them from being updated during training,

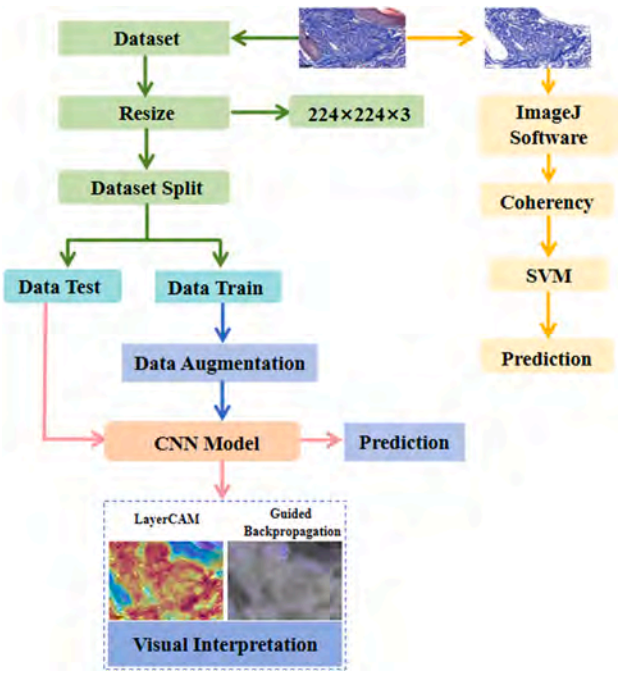

Fig. 2. The overall framework of the work. The left side of the figure shows the proposed visually interpretable CNN model for wound healing progression prediction, using LayerCAM and Guided Backpropagation to highlight critical image regions. On the right, the traditional method involves segmenting collagen fibers from wound images based on color properties, calculating coherency with ImageJ, and constructing an SVM model for healing prediction based on this coherency.

thereby reducing the risk of overfitting to our specific dataset. Subsequently, we added two custom fully connected layers on top of the frozen convolutional layers. The first fully connected layer was designed to further process the feature maps extracted by the convolutional layers, transforming them into a more abstract representation suitable for our specific task of wound healing progression assessment. The second fully connected layer served as the output layer, generating the final predictions for our task. Furthermore, we have incorporated a dropout layer between these two fully connected layers. By randomly deactivating a subset of neurons, this dropout layer prevents the model from becoming overly reliant on specific neurons, thereby enhancing its generalization capabilities and further reducing the likelihood of overfitting. This method we proposed is referred to as VGG16-7. Fig. 3 presents an overview of VGG16 and our proposed VGG16-7 method.

3.2.2. *Visual interpretation*

LayerCAM is an extension of CAM that generates more detailed visualizations by producing class activation maps at multiple layers of the CNN. The fundamental concept behind LayerCAM involves utilizing backward class-specific gradients to assign distinct weights to each spatial location in a feature map. The computation of gradients is shown in Equation (1), where y_c is the predicted score for the input image belonging to class c. A represents all the feature maps outputted by a specific layer of the model. A_{ij}^{k} denotes the feature value at the *i-th* row and *j-th* column of the *k-th* feature map, while g_{ij}^{kc} represents the gradient corresponding to that feature value.

$$g_{ij}^{kc} = \frac{\partial y^{c}}{\partial A_{ij}^{k}} \tag{1}$$

Positive gradients at a specific location in the feature map suggest that increasing the intensity of that location would positively influence the prediction score for the target class. In such cases, the corresponding gradients are used as weights. Conversely, locations with negative gradients are assigned a weight of zero, as intensifying them would negatively impact the prediction score.

The ReLU operation described in Equation (2) selectively preserves positive gradient values while setting negative gradient values to 0. In Equation (3), m_{ij}^{k} represents the class activation mapping value of A_{ij}^{k}. Finally, the class activation mapping M^{c} is obtained by performing a channel-wise sum of m^{k}, and the ReLU function is applied to retain positive activation values. By leveraging the LayerCAM technique, we

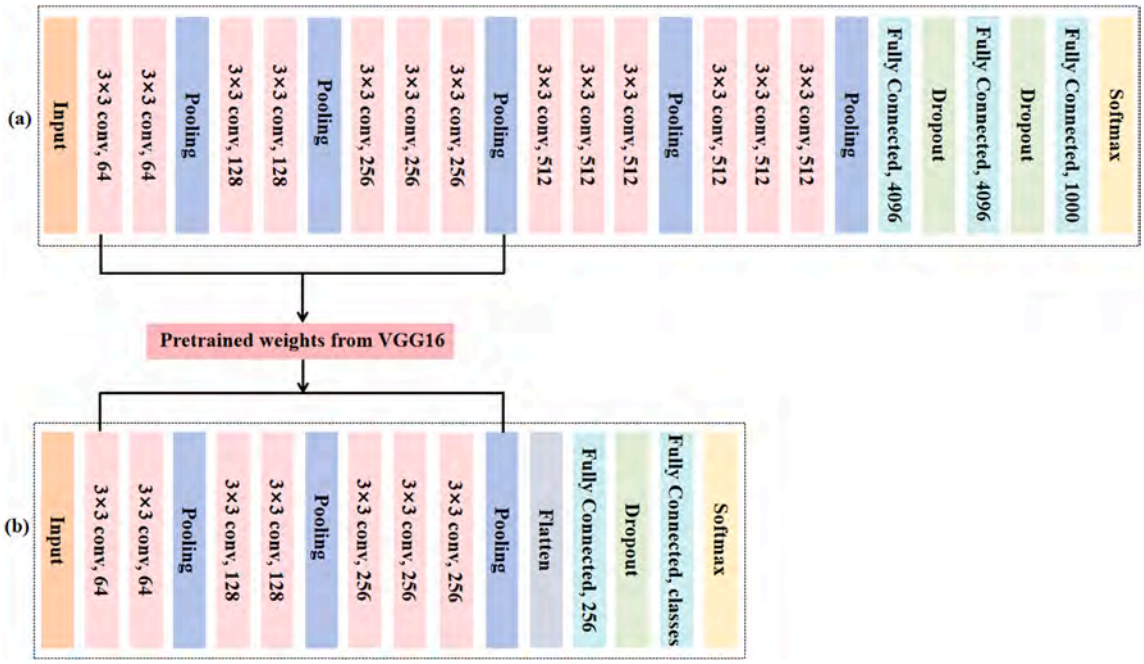

Fig. 3. (a) The VGG16 architecture features 13 convolutional layers for feature extraction and 3 fully connected layers for classification. (b) The customized VGG16-7 model, leveraging the first seven pre-trained convolutional layers of VGG16, is complemented by two newly designed fully connected layers (with the second layer tailored to match the input dataset's class count) and a dropout layer to mitigate overfitting.

are able to locate collagen regions from the layers of the model.

$$ReLU\left(g_{ij}^{kc}\right) = max\left(0, g_{ij}^{kc}\right) \tag{2}$$

$$m_{ij}^{k} = ReLU\left(g_{ij}^{kc}\right) \bullet A_{ij}^{k} \tag{3}$$

$$M^{c} = ReLU\sum_{k} m^{k} \tag{4}$$

Guided Backpropagation is a technique used to visualize and interpret the decision-making process of a convolutional neural network (CNN). Its purpose is to highlight the influential regions of an input image that have the most significant impact on the network's output prediction. The Guided Backpropagation method selectively propagates gradients where both the corresponding feature value and gradient value are positive, setting the gradient values to 0 for other positions. Compared to LayerCAM, the Guided Backpropagation can retain the fine-grained information of crucial pixels for the prediction. However, it is relatively weak in distinguishing subtle differences between different classes, lacking sensitivity to class-specific information and explicit discriminative ability, and may experience a decrease in interpretability accuracy as it may incorrectly highlight regions unrelated to the target class or portray them as important features.

To achieve more interpretable and comprehensive visualization results, we leverage the strengths of Guided Backpropagation and LayerCAM. We perform element-wise multiplication between the LayerCAM heatmap and the positive gradients computed by Guided Backpropagation to obtain the visualization result. Fig. 4 illustrates the mechanism of collagen visualization. This approach allows us to visualize the network's predictions for wound healing in a more comprehensive manner, taking advantage of accurate collagen localization and preserving fine-grained details. By combining these techniques, we enhance the interpretability and richness of the visualizations.

3.2.3. Traditional statistic analysis of collagen fiber orientation

The structural arrangement of collagen fibers varies significantly across different statuses of wound healing, and these variations are key to differentiating between the statuses. In normal skin tissue, collagen fibers are arranged in order to form neat fiber bundles, which enhances the coherence of its structure [7]. However, once the skin is damaged, the arrangement of collagen fibers in the wound area changes. In the early periods of wound healing, newly formed collagen fibers are shorter in length, smaller in diameter, and more randomly dispersed in arrangement, which results in lower coherence. In the later periods of healing, the collagen fibers gradually become denser, increase in diameter, lengthen, and become more orderly, which increases the coherency of collagen fibers [7].

To compare our method with the traditional method, we employed the traditional statistical method to analyze the coherency of collagen fibers in wound histological images. To quantify the coherency of collagen fiber orientation, we utilized the specialized software Fiji (version v1.54m) [60]. Fiji is an extension of the widely used image processing and analysis tool ImageJ, known for its multifunctionality in scientific research. Specifically, in the first step, we extract the blue regions representing collagen fibers from the histological images based on hue, saturation, and brightness to obtain segmentation masks, and then segment the collagen images from the histological images using these masks. In the second step, we open the collagen images with Fiji and use its Image menu to convert them into 16-bit format. In the third step, we use Fiji's OrientationJ plugin to calculate the coherency of collagen fiber orientation. Fig. 5 presents the workflow for the statistical analysis of collagen fiber orientation.

In this study, we utilized Python's numpy library to store coherency data and calculate metrics such as mean and quartiles [61]. Additionally, we employed Python's matplotlib library to create box plots that visually represent the distribution of these coherency data [62]. Furthermore, we conducted a *t*-test statistical analysis on the coherency using Python and its SciPy library's stats module [63].

4. Results

4.1. Network training and visual interpretability

When training the model on Dataset 1, which consists of five categories of skin images, the model was configured to produce five output classes. The learning rate was set to 0.00001, and the batch size was set to 20. For Dataset 2, which comprises three categories of skin images, the model's output was adjusted to three classes. In this case, the learning rate was increased to 0.0001, and the batch size was set to 30. Both datasets were trained for a total of 40 epochs, with the dropout set to 0.1. The training of the deep learning model was done on NVIDIA Corporation Device 2230 GPU, and the development environment includes version 3.8.0 of Python and version 1.8.1 of the PyTorch framework.

In evaluating the classification performance of our model, we employed a suite of metrics, including Accuracy (ACC), Area Under the Curve (AUC), Precision, Recall and F1 score. The respective calculations for these metrics are as follows:

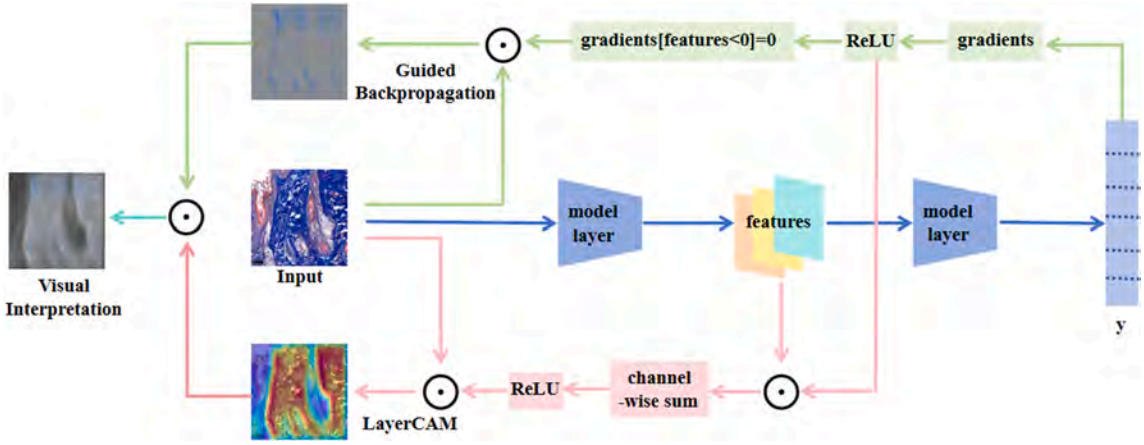

Fig. 4. Visualization framework. LayerCAM enhances CAM by creating detailed class activation maps across CNN layers, leveraging gradients to pinpoint collagen regions. Guided Backpropagation highlights influential image regions but may lack class specificity. Combining these techniques improves visualization interpretability and richness by accurately locating collagen and preserving fine details.

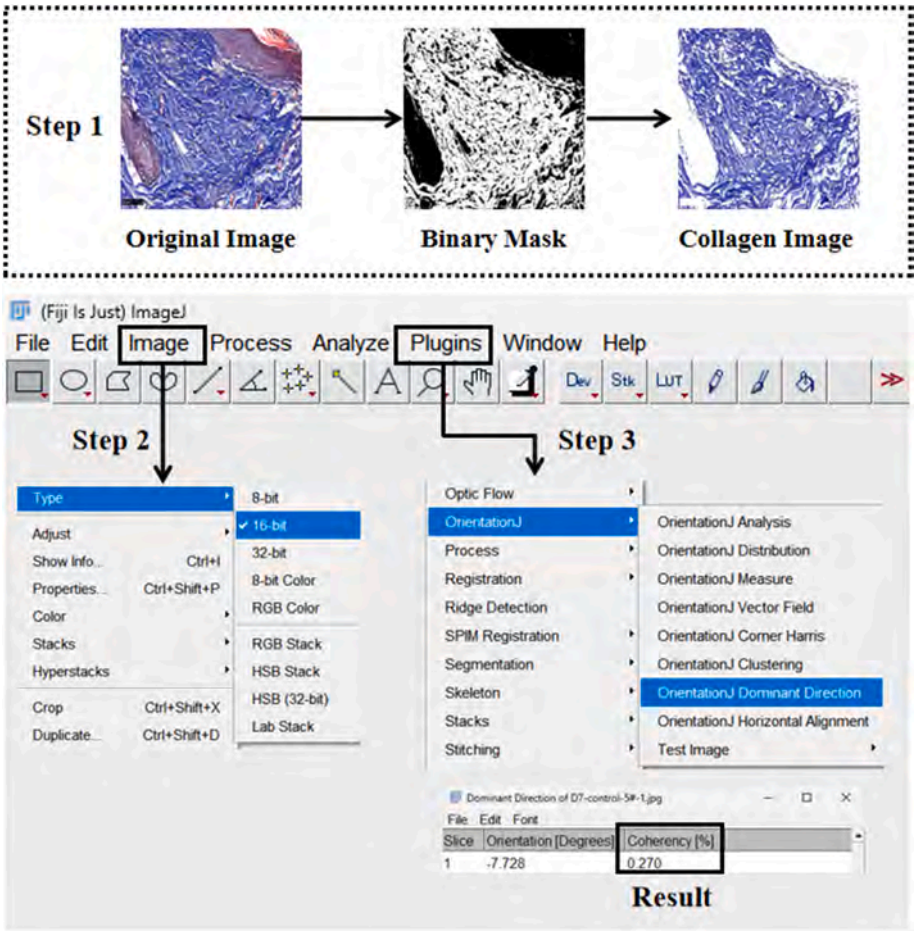

Fig. 5. Presentation of statistic analysis of collagen fiber orientation. Step 1: Extract collagen regions from histological images based on hue, saturation, and brightness. Step 2: Convert collagen images to 16-bit format using Fiji. Step 3: Calculate collagen fiber orientation coherency using Fiji's OrientationJ plugin.

$$ACC = \frac{TP + TN}{TP + TN + FP + FN}, \tag{5}$$

$$Precision = \frac{TP}{TP + FP}, \tag{6}$$

$$Recall = \frac{TP}{TP + FN}, \tag{7}$$

$$F1 = 2 \times \frac{Precision \times Recall}{Precision + Recall}, \tag{8}$$

where TP, TN, FP, and FN denote true positives, true negatives, false positives, and false negatives, respectively. AUC is calculated by plotting the True Positive Rate (TPR) against the False Positive Rate (FPR) at various threshold settings and measuring the area under the resulting curve.

Our proposed CNN model, VGG16-7, achieved classification results on the test sets of Dataset 1 with an accuracy of 0.85 ± 0.04, AUC of 0.96 ± 0.01, F1 score of 0.84 ± 0.04, precision of 0.87 ± 0.05, and recall of 0.85 ± 0.04. Table 5 presents the detailed experimental results. Similarly, on the test sets of Dataset 2, the model achieved an accuracy of 0.78 ± 0.06, AUC of 0.93 ± 0.02, F1 score of 0.77 ± 0.06, precision of 0.80 ± 0.06, and recall of 0.78 ± 0.06. Table 6 displays the detailed classification results for this dataset. The two bolded rows in Tables 5 and 6 demonstrate the mean and standard deviation of classification metrics for the training and test sets, generated by the VGG16-7 model through five-fold cross-validation on Dataset 1 and Dataset 2, respectively. The ACC curves, AUC curves, loss curves, and confusion matrices for model training on both datasets are presented in the supplementary file. These experimental results clearly demonstrate the excellent performance of our proposed model on skin wound datasets, highlighting

Table 5
Classification results of Dataset 1 by VGG16-7.

		ACC	AUC	F1 Score	Precision	Recall
Train	Data Split 1	0.90	0.99	0.90	0.90	0.90
	Data Split 2	0.91	0.99	0.91	0.91	0.91
	Data Split 3	0.88	0.99	0.88	0.88	0.88
	Data Split 4	0.89	1.00	0.89	0.90	0.89
	Data Split 5	0.86	0.97	0.82	0.87	0.86
	Mean ± Std	**0.89 ± 0.02**	**0.99 ± 0.01**	**0.88 ± 0.04**	**0.90 ± 0.02**	**0.89 ± 0.02**
Test	Data Split 1	0.89	0.97	0.89	0.92	0.89
	Data Split 2	0.85	0.98	0.84	0.88	0.85
	Data Split 3	0.80	0.95	0.80	0.81	0.80
	Data Split 4	0.87	0.96	0.87	0.88	0.87
	Data Split 5	0.83	0.95	0.82	0.88	0.83
	Mean ± Std	**0.85 ± 0.04**	**0.96 ± 0.01**	**0.84 ± 0.04**	**0.87 ± 0.05**	**0.85 ± 0.04**

Table 6
Classification results of Dataset 2 by VGG16-7.

		ACC	AUC	F1 Score	Precision	Recall
Train	Data Split 1	0.90	0.98	0.89	0.90	0.90
	Data Split 2	0.93	0.99	0.93	0.93	0.93
	Data Split 3	0.88	0.98	0.88	0.88	0.88
	Data Split 4	0.95	0.99	0.95	0.95	0.95
	Data Split 5	0.94	0.99	0.94	0.94	0.94
	Mean ± Std	**0.92 ± 0.03**	**0.99 ± 0.01**	**0.92 ± 0.03**	**0.92 ± 0.03**	**0.92 ± 0.03**
Test	Data Split 1	0.82	0.93	0.81	0.82	0.82
	Data Split 2	0.76	0.91	0.76	0.77	0.76
	Data Split 3	0.72	0.91	0.70	0.75	0.72
	Data Split 4	0.86	0.93	0.86	0.90	0.86
	Data Split 5	0.74	0.95	0.73	0.77	0.74
	Mean ± Std	**0.78 ± 0.06**	**0.93 ± 0.02**	**0.77 ± 0.06**	**0.80 ± 0.06**	**0.78 ± 0.06**

its capability to assess wound healing progression.

Additionally, we employed Guided Backpropagation and LayerCAM techniques to accurately localize the regions of interest (ROI) in the images. Fig. 6 offers visual interpretability examples for all categories in Dataset 1, while Fig. 7 presents visual interpretability examples for all classes within Dataset 2. This analysis demonstrated that our model specifically focused on learning the collagen fibers of histological images for classifying the statuses of wound healing rather than other tissue structures, such as cells, which hold less biomedical significance in the context of wound healing. Since the histological images of the wound tissues at different healing statuses exhibit variations not only in the collagen fibers stained in blue but also in the appendages stained in red or purple (such as hair follicles, sweat glands, and sebaceous glands), it is essential for the deep learning model to prioritize the collagen fibers. This ensures that the model's prediction of the status of wound healing is based on biologically significant collagen fibers. In addition, the interpretable framework highlights the most relevant part of the histological image with the model prediction, namely the collagen region, through the superposition of the class activation heat map and the original map without pixel-level labels. This approach not only confirmed the accuracy of the model but also allowed doctors to delineate collagen areas associated with wound healing without spending a lot of time on manual labeling.

In summary, by utilizing deep learning-based image analysis techniques, our model can identify subtle changes in collagen fibers at different statuses of wound healing. This allows the model to more accurately predict the progress of healing and identify any deviations from the norm, such as delayed healing. In addition, the visual interpretability of our model enables researchers and clinicians to understand the decision-making process behind the model's predictions by activating regions in the input images that are relevant to the predictions.

4.2. Quantification of collagen fiber orientation

We quantitatively assess the coherency of collagen fibers in the histological images from Dataset 1and Dataset 2, following the methodologies outlined in Section 3.2.3. The distribution of coherency for

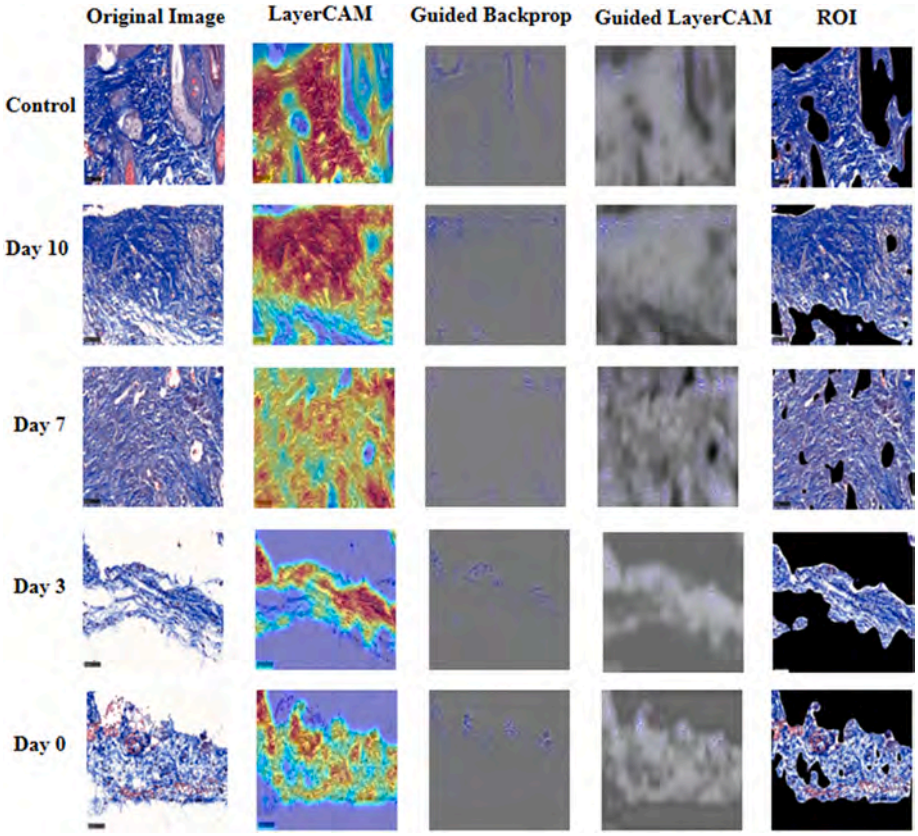

Fig. 6. Visual interpretability examples of Dataset 1, showing original wound histological images, LayerCAM class activation maps, collagen images influencing model decisions via Guided Backpropagation, collagen regions obtained by combining LayerCAM and Guided Backpropagation, and segmented Regions of Interest (ROI) based on these collagen regions.

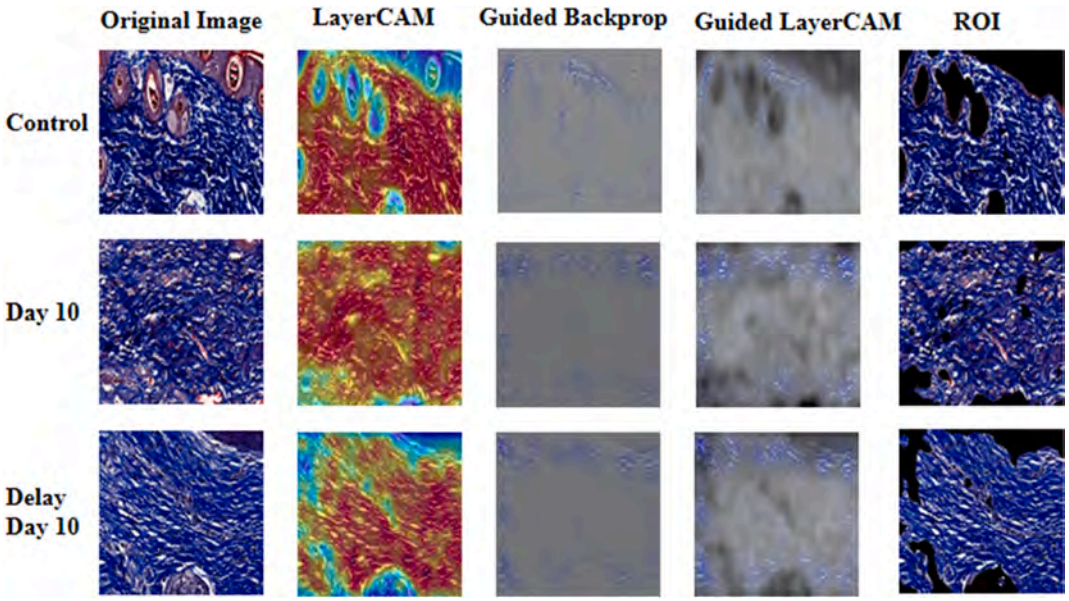

Fig. 7. Visual interpretability examples of Dataset 2, showing original wound histological images, LayerCAM class activation maps, collagen images influencing model decisions via Guided Backpropagation, collagen regions obtained by combining LayerCAM and Guided Backpropagation, and segmented Regions of Interest (ROI) based on these collagen regions.

each dataset is represented by the box plots shown in Figs. 8 and 9. Table 7, Tables 9, and Table 11 present the mean, median, standard deviation, first quartile (Q1), and third quartile (Q3) of the coherency values for the two datasets. We employ the quartile method to detect outliers within the coherency dataset. By calculating the first quartile (Q1) and the third quartile (Q3), and determining the interquartile range (IQR) between them, we establish the normal range for the coherency data and flag any data points lying outside this range as outliers. Figs. 8 and 9 reveal that the coherency of collagen fibers gradually increases during the healing process. During the early periods of wound healing (Day 0, Day 3), the coherency of collagen fibers in the wound tissue is lower compared to that in normal tissue (Control). This suggests that in the initial phases, the collagen fibers in the normal tissue exhibit a higher degree of alignment and organization compared to the wound tissue. However, in the later periods of wound healing, such as on the 10th day of wound healing (Day 10), the coherency of collagen fibers in the wound tissue surpasses that of normal tissue. Additionally, it is evident that the within-group standard deviation of coherency is high. This suggests that samples within the same group exhibit diverse patterns of collagen fiber orientation. Moreover, Fig. 9 shows that the delayed wound healing tissue (Delay Day 10) exhibits higher coherency values compared to the other groups. This finding suggests that in cases of delayed wound healing, there is a more pronounced alignment and organization of collagen fibers. This may indicate a high potential for scar formation in diabetic wounds [7,64,65]. Furthermore, by referring to Tables 9 and 11, we can observe significant variations in coherency values across different batches of Dataset 2. For instance, even within the normal skin, the mean coherency for the first batch is 0.0604, while for the second batch, it is 0.12.

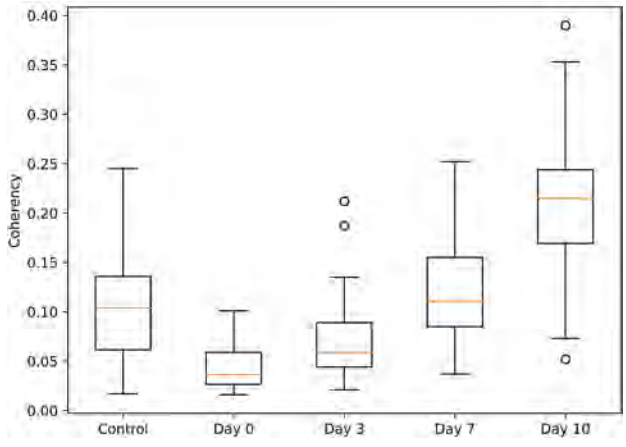

Fig. 8. Coherency of collagen in Dataset 1. As healing progresses, the coherency of collagen progressively increases, surpassing that of the Control group by the seventh day of wound healing.

We also performed t-tests to determine the significance of differences in collagen fiber coherency among different categories of histological images within Dataset 1and within batches of Dataset 2, respectively, as shown in Table 8, Tables 10, and Table 12. Upon examining these tables, we can observe that in some cases, the p-values are greater than 0.05, indicating that there is no significant difference between some groups.

Based on the above observations, we further confirm that traditional quantification methods have three disadvantages. First, there is a lack of clear threshold standards, so we cannot distinguish the statuses of wound healing through the values of these indicators. Second, there is often a high within-group variance that might make assessment of individual wounds difficult. Third, there is no significant difference between some groups. These limitations hinder traditional quantitative methods from serving as reliable assessments of wound healing progress.

To elucidate the constraints associated with traditional metrics, we leveraged previously acquired coherence data to train a Support Vector Machine (SVM) model [25], aiming to develop a classifier adept at distinguishing various statuses of wound healing. To ensure a fair comparison, both the SVM model and our proposed deep learning model, VGG16-7, adhered to the same data partitioning strategy—five-fold cross-validation. Nonetheless, during the testing phase, the SVM's performance on the two datasets (Dataset 1and Dataset 2) fell short of expectations, with accuracy rates of 52 % and 39 %, respectively, as detailed in Tables 13 and 14. In Tables 13 and 14, the bolded rows present the mean ± standard deviation of classification performance for training and test sets, produced via the SVM framework by applying five-fold cross-validation to collagen coherency data in Dataset 1 and Dataset 2, respectively. In stark contrast, our novel deep learning model, VGG16-7, exhibited remarkable accuracy rates of 85 % and 78 %

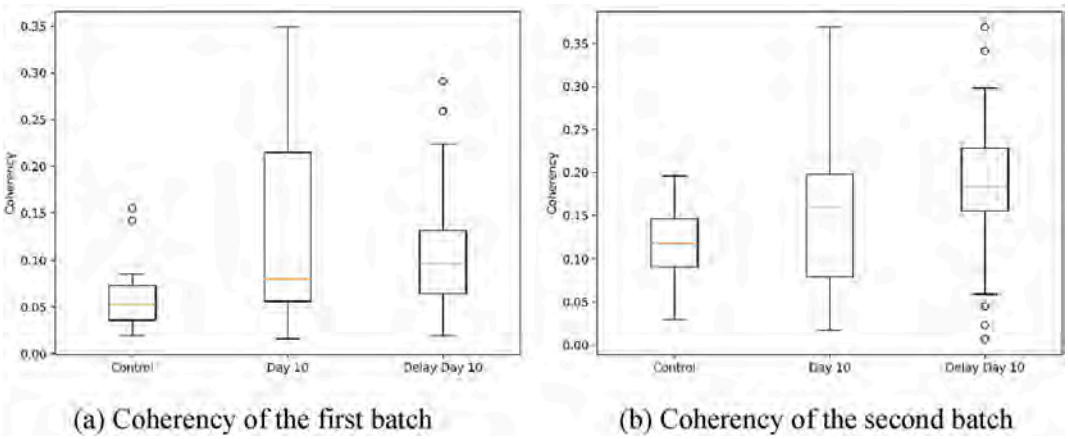

Fig. 9. Coherency of collagen in Dataset 2. The coherency of collagen in skin wounds with delayed healing (Delay Day 10) is higher than that of collagen in normal skin wounds (Day 10) at the same time point, as well as compared to the normal skin (Control).

Table 7
Coherency of collagen in Dataset 1.

Classes	Mean	Median	Standard Deviation	First Quartile (Q1)	Third Quartile (Q3)
Control	0.106	0.104	0.05	0.062	0.136
Day 0	0.046	0.036	0.028	0.027	0.059
Day 3	0.08	0.059	0.054	0.044	0.089
Day 7	0.126	0.111	0.056	0.085	0.155
Day 10	0.21	0.215	0.07	0.169	0.244

Table 8
The p-value of the *t*-test for coherency in Dataset 1.

	Control	Day0	Day3	Day7	Day10
Control	-	0.0005	0.1320	0.1651	0.0000
Day0	0.0005	-	0.0707	0.0000	0.0000
Day3	0.1320	0.0707	-	0.0132	0.0000
Day7	0.1651	0.0000	0.0132	-	0.0000
Day10	0.0000	0.0000	0.0000	0.0000	-

Table 9
Coherency of collagen in the first batch of Dataset 2.

Classes	Mean	Median	Standard Deviation	First Quartile (Q1)	Third Quartile (Q3)
Control	0.06	0.053	0.034	0.036	0.073
Day 10	0.127	0.08	0.108	0.056	0.215
Delay Day 10	0.107	0.096	0.064	0.064	0.132

Table 10
The p-value of the *t*-test for coherency of collagen in the first batch of Dataset 2.

	Control	Day 10	Delay day 10
Control	-	0.0119	0.0042
Day 10	0.0119	-	0.3941
Delay day 10	0.0042	0.3941	-

on these datasets. This further demonstrates that, while traditional metrics may still be effective in certain situations for assessing wound healing progress, our proposed deep learning model, VGG16-7, is capable of providing more accurate and reliable classification results.

Table 11
Coherency of collagen in the second batch of Dataset 2.

Classes	Mean	Median	Standard Deviation	First Quartile (Q1)	Third Quartile (Q3)
Control	0.12	0.118	0.044	0.09	0.146
Day 10	0.151	0.16	0.084	0.079	0.198
Delay Day 10	0.186	0.184	0.081	0.155	0.228

Table 12
The p-value of the *t*-test for coherency collagen in the second batch of Dataset 2.

	Control	Day 10	Delay day 10
Control	-	0.1054	0.0010
Day 10	0.1054	-	0.0760
Delay day 10	0.0010	0.0760	-

Table 13
Classification results of Dataset 1 by SVM.

		ACC	AUC	F1 Score	Precision	Recall
Train	Data Split 1	0.59	0.78	0.54	0.63	0.59
	Data Split 2	0.56	0.82	0.53	0.54	0.56
	Data Split 3	0.56	0.77	0.64	0.5	0.56
	Data Split 4	0.56	0.73	0.51	0.61	0.56
	Data Split 5	0.57	0.79	0.55	0.57	0.57
	Mean ± Std	**0.57 ± 0.01**	**0.78 ± 0.03**	**0.55 ± 0.05**	**0.57 ± 0.05**	**0.57 ± 0.01**
Test	Data Split 1	0.44	0.78	0.4	0.5	0.44
	Data Split 2	0.56	0.73	0.65	0.53	0.56
	Data Split 3	0.48	0.63	0.46	0.56	0.48
	Data Split 4	0.60	0.71	0.57	0.72	0.60
	Data Split 5	0.50	0.73	0.48	0.54	0.50
	Mean ± Std	**0.52 ± 0.06**	**0.72 ± 0.05**	**0.51 ± 0.10**	**0.57 ± 0.09**	**0.52 ± 0.06**

Table 14
Classification results of Dataset 2 by SVM.

		ACC	AUC	F1 Score	Precision	Recall
Train	Data Split 1	0.49	0.7	0.45	0.49	0.49
	Data Split 2	0.49	0.64	0.48	0.48	0.49
	Data Split 3	0.49	0.65	0.46	0.48	0.49
	Data Split 4	0.51	0.43	0.49	0.57	0.51
	Data Split 5	0.51	0.68	0.5	0.52	0.51
	Mean ± Std	**0.50 ± 0.01**	**0.61 ± 0.11**	**0.48 ± 0.02**	**0.51 ± 0.04**	**0.50 ± 0.01**
Test	Data Split 1	0.34	0.51	0.54	0.29	0.34
	Data Split 2	0.37	0.54	0.37	0.38	0.37
	Data Split 3	0.46	0.55	0.44	0.51	0.46
	Data Split 4	0.43	0.50	0.63	0.35	0.43
	Data Split 5	0.37	0.57	0.36	0.36	0.37
	Mean ± Std	**0.39 ± 0.05**	**0.53 ± 0.03**	**0.39 ± 0.05**	**0.38 ± 0.08**	**0.39 ± 0.05**

5. Discussion

Through detailed quantitative analysis of collagen fiber orientation, we have observed that as the wound healing process progresses, the arrangement of collagen fibers in the wound tissue gradually transitions from disorganized and chaotic to a more orderly and coherent pattern. This increased coherency implies an important shift in structural reconstruction and functional recovery during wound healing.

It is noteworthy that the coherency change in collagen fibers may not always be significant at various statuses of wound healing. Especially when comparing the various statuses of wound healing or analyzing the healing delay caused by pathological conditions such as diabetes, traditional methods may not fully reveal the subtle differences in collagen fiber arrangement to reach the expected goal. Even when we input the coherency values corresponding to collagen fibers into the machine learning model, we achieve only low accuracy, which further highlights the limitations of traditional methods in accuracy and sensitivity, which may not fully identify the small changes in collagen fiber arrangement that are critical for accurately determining the specific status of wound healing and evaluating treatment effectiveness. As a result, the validity of these traditional methods as reliable criteria for assessing wound healing progression may be questioned. This prompted us to explore more advanced techniques to capture these changes more accurately and comprehensively, thus providing a more reliable basis for the assessment of wound healing.

The advanced performance of our deep learning model in image recognition and feature extraction provides a more accurate and sensitive identification method for wound healing assessment. This method is particularly good at picking up subtle changes that traditional statistical methods might miss, especially in cases of delayed healing. For example, by feeding histological images of diabetic wound skin at 10 days into our model, it is able to identify features that do not match the normal healing trajectory and accurately classify these samples as delayed healing. This prompt feedback is extremely valuable for medical professionals as it allows them to intervene in a timely manner to optimize treatment strategies to facilitate a smooth recovery from the wound. This capability significantly improves the ability to process complex biomedical data beyond the limitations of traditional statistical methods. In addition, our model enhances the visualization and transparency of its decision-making process by labeling the region of interest (ROI) on the histological images. This visualization approach not only helps researchers and medical professionals gain insight into the model's classification decisions but also enhances the credibility and reliability of the model's output.

Compared to traditional collagen quantification methods, our proposed deep learning-based model offers a more accurate and visually interpretable assessment of wound tissue healing. This multi-angle analysis gives healthcare professionals more sophisticated monitoring tools, enabling them to quickly grasp the dynamics of wound healing and adjust treatment when necessary, especially in the face of complex or slow-healing wound cases, to monitor and intervene in a timely manner, thereby improving the speed of patient recovery.

6. Conclusion

In our study, we collected two skin wound datasets and proposed a deep learning approach to classify histological images of normal and wounded skin tissues, aiming to accurately assess the different statuses of wound healing. This method achieved accuracy rates of 85 % and 78 % on the two datasets, respectively. This advance effectively overcomes the shortcomings of traditional quantitative analyses in distinguishing the status of wound healing, as it is often difficult to make accurate judgments based solely on quantitative results of the spatial properties of collagen fibers. In addition, our approach combines Guided Backpropagation and LayerCAM techniques to build an interpretability framework that provides a visual interpretation of the model. The framework can accurately identify the spatial distribution of collagen associated with predictions without manual pixel-level annotations. This shows that our model focuses on learning collagen regions that have biological significance for predicting the progress of wound healing rather than other less indicative structures, revealing the transparency and reliability of the model's predicted results. In summary, we provide medical professionals with tools to monitor the extent of wound healing and help them adjust their treatment plan in time.

In the future, we plan to use second harmonic generation (SHG) imaging to obtain collagen images of wounds to further improve the accuracy of prediction of wound healing progress. SHG technology can capture high-resolution images of collagen fibers in a non-invasive manner, which is advantageous for models to learn about changes in collagen during wound healing. Our goal is to develop tools that can more accurately monitor the wound healing process, provide more solid support for clinical treatment, and also provide new ways to further explore the pathological mechanisms of abnormal conditions of wound healing, such as delayed healing.

CRediT authorship contribution statement

Juan He: Writing – original draft, Visualization, Methodology. **Xiaoyan Wang:** Formal analysis, Data curation. **Zhengshan Wang:** Writing – review & editing. **Ruitao Xie:** Writing – review & editing, Validation. **Zhiming Zhang:** Data curation. **Tzu-Ming Liu:** Data curation. **Yunpeng Cai:** Writing – review & editing, Supervision. **Long Chen:** Writing – review & editing, Supervision, Project administration.

Ethics statement

All animal experiments complied with the University of Macau's Sub-panel on Animal Research Ethics (UMARE - 019–2022). Male nude mice used for the experiments, aged between 6 and 8 weeks and weighed in a weight range of 20–23 g, were provided by the Animal Laboratory Facilities of the University of Macau. During the experimental procedure, anesthesia was administered to alleviate the suffering of the animals.

Declaration of competing interest

The authors affirm that there are no competing financial interests or

personal affiliations that might be perceived as affecting the research findings presented in this paper.

Acknowledgment

This work was supported by the Guangdong-Hong Kong-Macao Joint Innovation Project under Grant 2023A0505030016, the Science and Technology Development Fund, Macao S.A.R under Grant 0046/2023/RIA1, the University of Macau and the University of Macau Development Foundation under Grant MYRG-GRG2023-00106-FST-UMDF.

Appendix A. Supplementary data

Supplementary data to this article can be found online at https://doi.org/10.1016/j.compbiomed.2025.110110.

References

[1] S.S. Mathew-Steiner, S. Roy, C.K. Sen, Collagen in wound healing, Bioengineering 8 (5) (2021) 63.
[2] J.D. Jones, M.R. Rodriguez, K.P. Quinn, Automated extraction of skin wound healing biomarkers from in vivo label-free multiphoton microscopy using convolutional neural networks, Laser Surg. Med. 53 (8) (2021) 1086–1095.
[3] A. Suvik, A.W.M. Effendy, The use of modified Masson's trichrome staining in collagen evaluation in wound healing study, Mal. J. Vet. Res. 3 (1) (2012) 39–47.
[4] F. Fereidouni, A. Todd, Y. Li, Dual-mode emission and transmission microscopy for virtual histochemistry using hematoxylin-and-eosin-stained tissue sections, Biomed. Opt. Express 10 (12) (2019) 6516–6530.
[5] P.J. Campagnola, L.M. Loew, Second-harmonic imaging microscopy for visualizing biomolecular arrays in cells, tissues, and organisms, Nat. Biotechnol. 21 (11) (2003) 1356–1360.
[6] Y. Liu, A. Keikhosravi, C.A. Pehlke, Fibrillar collagen quantification with curvelet transform based computational methods, Front. Bioeng. Biotechnol. 8 (2020) 198.
[7] T.D. Clemons, M. Bradshaw, P. Toshniwal, Coherency image analysis to quantify collagen architecture: implications in scar assessment, RSC Adv. 8 (18) (2018) 9661–9669.
[8] K.P. Quinn, A. Golberg, G.F. Broelsch, An automated image processing method to quantify collagen fibre organization within cutaneous scar tissue, Exp. Dermatol. 24 (1) (2015) 78–80.
[9] S. Suganyadevi, V. Seethalakshmi, K. Balasamy, A review on deep learning in medical image analysis, Int. J. Multimedia Inf. Retrieval 11 (1) (2022) 19–38.
[10] R. Wang, T. Lei, R. Cui, Medical image segmentation using deep learning: a survey, IET Image Process. 16 (5) (2022) 1243–1267.
[11] H.P. Chan, R.K. Samala, L.M. Hadjiiski, Deep learning in medical image analysis, in: Deep Learning in Medical Image Analysis: Challenges and Applications, 2020, pp. 3–21.
[12] S. Xie, Z. Yu, Z. Lv, Multi-disease prediction based on deep learning: a survey, CMES-Comput. Model, Eng. Sci. 128 (2) (2021).
[13] R. Gupta, D. Srivastava, M. Sahu, Artificial intelligence to deep learning: machine intelligence approach for drug discovery, Mol. Divers. 25 (2021) 1315–1360.
[14] T.T.A. Pham, H. Kim, Y. Lee, Deep learning for analysis of collagen fiber organization in scar tissue, IEEE Access 9 (2021) 101755–101764.
[15] T.T.A. Pham, H. Kim, Y. Lee, Universal convolutional neural network for histology-independent analysis of collagen fiber organization in scar tissue, IEEE Access 10 (2022) 34379–34392.
[16] H. Carrión, M. Jafari, H.Y. Yang, Healnet-self-supervised acute wound heal-stage classification, in: Int. Workshop Mach. Learn. Med. Imaging, Springer Nature Switzerland, Cham, 2022, pp. 446–455.
[17] L. Wang, M. Zhou, T. Xu, Multifunctional hydrogel as wound dressing for intelligent wound monitoring, Chem. Eng. J. 433 (2022) 134625.
[18] F. Zhuang, Z. Qi, K. Duan, A comprehensive survey on transfer learning, Proc. IEEE 109 (1) (2020) 43–76.
[19] S. Niu, Y. Liu, J. Wang, A decade survey of transfer learning (2010–2020), IEEE Trans. Artif. Intell. 1 (2) (2020) 151–166.
[20] K. Simonyan, A. Zisserman, Very deep convolutional networks for large-scale image recognition, arXiv preprint arXiv:1409.1556 (2014). https://doi.org/10.48550/arXiv.1409.1556.
[21] J. Deng, W. Dong, R. Socher, Imagenet: a large-scale hierarchical image database, in: 2009 IEEE Conf. Comput. Vis. Pattern Recognit., IEEE, 2009, pp. 248–255.
[22] P.T. Jiang, C.B. Zhang, Q. Hou, Layercam: exploring hierarchical class activation maps for localization, IEEE Trans. Image Process. 30 (2021) 5875–5888.
[23] J.T. Springenberg, A. Dosovitskiy, T. Brox, Striving for simplicity: the all convolutional net, arXiv preprint arXiv:1412.6806 (2014). https://doi.org/10.48550/arXiv.1412.6806.
[24] R.R. Selvaraju, M. Cogswell, A. Das, Grad-CAM: visual explanations from deep networks via gradient-based localization, in: Proc. IEEE Int. Conf. Comput. Vis., 2017, pp. 618–626.
[25] C. Cortes, V. Vapnik, Support-vector network, Mach. Learn. 20 (1995) 273–297.
[26] R.E. Rodrigues, N. Kosaric, C.A. Bonham, Wound healing: a cellular perspective, Physiol. Rev. 99 (1) (2019) 665–706.
[27] R.E. Burgeson, J.Z. Hollister, Collagen structure and its role in the body, in: R. E. Burgeson, J.Z. Hollister (Eds.), Biochemistry and Physiology of Collagen, Wiley-Blackwell, 2010, pp. 1–14.
[28] B. Gawronska-Kozak, K.T. Ilieva, Collagen and collagenase in wound healing, Methods Mol. Biol. 1043 (2013) 341–358.
[29] G.S. Schultz, G.A. Chin, L. Moldawer, Principles of wound healing, in: Mechanisms of Vascular Disease: A Reference Book for Vascular Specialists [Internet], University of Adelaide Press, Adelaide (AU), 2011, p. 23.
[30] S. Guo, L.A. DiPietro, Factors affecting wound healing, J. Dent. Res. 89 (3) (2010) 219–229.
[31] G.C. Gurtner, S. Werner, Y. Barrandon, et al., Wound repair and regeneration, Nature 453 (7193) (2008) 314–321.
[32] A. Das, M. Abas, N. Biswas, et al., A modified collagen dressing induces transition of inflammatory to reparative phenotype of wound macrophages, Sci. Rep. 9 (1) (2019) 14293.
[33] A. Das, S. Datta, E. Roche, et al., Novel mechanisms of Collagenase Santyl Ointment (CSO) in wound macrophage polarization and resolution of wound inflammation, Sci. Rep. 8 (1) (2018) 1696.
[34] R.G. Rosique, M.J. Rosique, J.A. Farina Junior, Curbing inflammation in skin wound healing: a review, Int. J. Inflamm. 2015 (1) (2015) 316235.
[35] M. Marchand, C. Monnot, L. Muller, et al., Extracellular matrix scaffolding in angiogenesis and capillary homeostasis, in: Seminars in Cell & Developmental Biology, Academic Press, 2019, pp. 147–156.
[36] T. Twardowski, A. Fertala, J. Orgel, et al., Type I collagen and collagen mimetics as angiogenesis promoting superpolymers, Curr. Pharm. Des. 13 (35) (2007) 3608–3621.
[37] A. Kisling, R.M. Lust, L.C. Katwa, What is the role of peptide fragments of collagen I and IV in health and disease? Life Sci. 228 (2019) 30–34.
[38] S. Ricard-Blum, The collagen family, cold spring harb, Perspect. Biol. 3 (1) (2011) a004978.
[39] S. Ricard-Blum, L. Ballut, Matricryptins derived from collagens and proteoglycans, Front. Biosci. 16 (1) (2011) 674–697.
[40] L. Liang, M. Liu, W. Sun, A deep learning approach to estimate chemically-treated collagenous tissue nonlinear anisotropic stress-strain responses from microscopy images, Acta Biomater. 63 (2017) 227–235.
[41] L. Schmarje, C. Zelenka, U. Geisen, et al., 2D and 3D segmentation of uncertain local collagen fiber orientations in SHG microscopy, in: German Conference on Pattern Recognition, Springer International Publishing, Cham, 2019, pp. 374–386.
[42] D. Paredes, P. Prasanna, C. Preece, et al., Automated assessment of the curliness of collagen fiber in breast cancer, in: Computer Vision–ECCV 2020 Workshops: Glasgow, UK, August 23–28, 2020, Part I 16, Springer International Publishing, 2020, pp. 267–279.
[43] A. Sneider, A. Kiemen, J.H. Kim, et al., Deep learning identification of stiffness markers in breast cancer, Biomaterials 285 (2022) 121540.
[44] W. Jiang, H. Wang, W. Chen, et al., Association of collagen deep learning classifier with prognosis and chemotherapy benefits in stage II–III colon cancer, Bioeng. Transl. Med. (2023) e10526.
[45] A.E. Woessner, K.P. Quinn, Improved segmentation of collagen second harmonic generation images with a deep learning convolutional neural network, J. Biophot. 15 (12) (2022) e202200191.
[46] N. Riberti, M. Furlani, E. D'Amico, et al., Deep learning for microstructural characterization of synchrotron radiation-based collagen bundle imaging in peri-implant soft tissues, Appl. Sci. 13 (7) (2023) 4423.
[47] H. Park, B. Li, Y. Liu, et al., Collagen fiber centerline tracking in fibrotic tissue via deep neural networks with variational autoencoder-based synthetic training data generation, Med. Image Anal. 90 (2023) 102961.
[48] R. Azad, et al., Medical image segmentation review: the success of U-Net, IEEE Trans. Pattern Anal. Mach. Intell. 46 (12) (2024) 10076–10095.
[49] C. Wang, X. Yan, M. Smith, et al., A unified framework for automatic wound segmentation and analysis with deep convolutional neural networks, in: 2015 37th Annual International Conference of the IEEE Engineering in Medicine and Biology Society (EMBC), IEEE, 2015, pp. 2415–2418.
[50] C. Wang, D.M. Anisuzzaman, V. Williamson, et al., Fully automatic wound segmentation with deep convolutional neural networks, Sci. Rep. 10 (1) (2020) 21897.
[51] J.D. Jones, M.R. Rodriguez, K.P. Quinn, Automated extraction of skin wound healing biomarkers from in vivo label-free multiphoton microscopy using convolutional neural networks, Laser Surg. Med. 53 (8) (2021) 1086–1095.
[52] D. Doğru, M.A. Özdemir, G.D. Özdemir, et al., A deep learning pipeline for the segmentation of in vitro wound healing microscopy images following laser therapy, in: 2022 Medical Technologies Congress (TIPTEKNO), IEEE, 2022, pp. 1–5.
[53] D. Doğru, G.D. Özdemir, M.A. Özdemir, et al., An automated in vitro wound healing microscopy image analysis approach utilizing U-net-based deep learning methodology, BMC Med. Imag. 24 (1) (2024) 158.
[54] M.D. Abràmoff, P.J. Magalhães, S.J. Ram, Image processing with ImageJ, Biophot. Int. 11 (7) (2004) 36–42.
[55] T. Gebäck, M.M.P. Schulz, P. Koumoutsakos, et al., TScratch: a novel and simple software tool for automated analysis of monolayer wound healing assays, Biotechniques 46 (4) (2009) 265–274.
[56] M. Schlereth, D. Stromer, Y. Mantri, et al., Initial investigations towards non-invasive monitoring of chronic wound healing using deep learning and ultrasound imaging, in: Bildverarbeitung für die Medizin 2022: Proceedings, German Workshop on Medical Image Computing, Heidelberg, June 26-28, 2022, Springer Fachmedien Wiesbaden, Wiesbaden, 2022, pp. 261–266.
[57] V.N. Shenoy, E. Foster, L. Aalami, et al., Deepwound: automated postoperative wound assessment and surgical site surveillance through convolutional neural

networks, in: 2018 IEEE International Conference on Bioinformatics and Biomedicine (BIBM), IEEE, 2018, pp. 1017–1021.
[58] R. Mousa, E. Matbooe, H. Khojasteh, Multi-modal wound classification using wound image and location by Xception and Gaussian Mixture Recurrent Neural Network (GMRNN), Preprints (2025), https://doi.org/10.20944/preprints202501.0655.v1.
[59] X. Wang, B. Jiang, H. Sun, et al., Noninvasive application of mesenchymal stem cell spheres derived from hESC accelerates wound healing in a CXCL12-CXCR4 axis-dependent manner, Theranostics 9 (21) (2019) 6112.
[60] J. Schindelin, I. Arganda-Carreras, E. Frise, et al., Fiji: an open-source platform for biological-image analysis, Nat. Methods 9 (7) (2012) 676–682.
[61] C.R. Harris, K.J. Millman, S.J. Van Der Walt, et al., Array programming with NumPy, Nat 585 (7825) (2020) 357–362.
[62] E. Bisong, E. Bisong, Matplotlib and seaborn, in: Building Machine Learning and Deep Learning Models on Google Cloud Platform: A Comprehensive Guide for Beginners, 2019, pp. 151–165.
[63] P. Virtanen, R. Gommers, T.E. Oliphant, et al., SciPy 1.0: fundamental algorithms for scientific computing in Python, Nat. Methods 17 (3) (2020) 261–272.
[64] O.A. Peña, P. Martin, Cellular and molecular mechanisms of skin wound healing, Nat. Rev. Mol. Cell Biol. (2024) 1–18.
[65] D. Correa-Gallegos, D. Jiang, S. Christ, et al., Patch repair of deep wounds by mobilized fascia, Nature 576 (7786) (2019) 287–292.